DFT Study of Polyaniline and Metal Composites as Nonprecious Metal Catalysts for Oxygen Reduction in Fuel Cells

ARTICLE *in* THE JOURNAL OF PHYSICAL CHEMISTRY C · OCTOBER 2012

Impact Factor: 4.77 · DOI: 10.1021/jp307055j

5 AUTHORS, INCLUDING:

Fan Li
Beijing University of Technology
39 PUBLICATIONS **277** CITATIONS

THE JOURNAL OF PHYSICAL CHEMISTRY C

Article

pubs.acs.org/JPCC

DFT Study of Polyaniline and Metal Composites as Nonprecious Metal Catalysts for Oxygen Reduction in Fuel Cells

Xin Chen,[†] Shaorui Sun,*[,†] Xiayan Wang,[†] Fan Li,[†] and Dingguo Xia*[,‡]

[†]College of Environmental and Energy Engineering, Beijing University of Technology, Beijing 100124, China

[‡]College of Engineering, Peking University, Beijing 100871, China

ABSTRACT: A theoretical study on the oxygen reduction mechanism catalyzed by metal−polyaniline is investigated in detail by means of density functional theory. In the oxygen reduction process, we find that −OH, not H_2O_2, is the reaction intermediate. The catalytic activities for the studied models decrease in the sequence CoFe−PANI > Fe−PANI (FeFe−PANI) > Co−PANI. This is due to a synergistic effect between heterogeneous metal atoms in CoFe−PANI, which facilitates additional electron donation from the active sites to the adsorbed oxygen reduction intermediates. The doping with cobalt may also decrease the HOMO−LUMO gap in CoFe−PANI, making it more active.

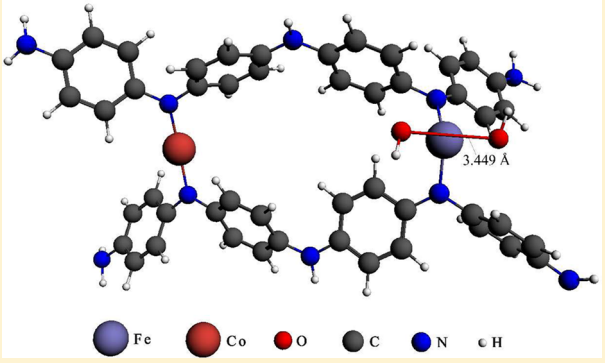

1. INTRODUCTION

Polymer electrolyte fuel cells (PEFCs) are regarded as one of the most promising candidates for stationary and mobile power generation due to their large energy yield and the low environmental impact of hydrogen oxidation. However, the cost of platinum (Pt) or Pt alloys serving as catalysts is prohibitive in PEFC in light of the high loading levels that are required for the oxygen reduction reaction (ORR).[1] Consequently, the development of nonprecious metal catalysts (NPMCs) with high ORR activity and durability is a major focus of PEFC research.[2−5] Recently, Fe/Co−N_x materials have revealed their great potential as one type of NPMC. Although impressive advances have been recently achieved, the understanding of the origin of the catalytic activity in Fe/Co−N_x materials is far from complete.

For Fe/Co−N_x-based NPMCs, there generally are a number of large challenges encountered in determining the structure of the active sites. First, metal atoms may either be at the center of the active sites, or they may merely serve to catalyze the formation of the active sites from carbon and nitrogen.[6−9] Second, the number of active sites is very sparse relative to the number of sites in the whole system, which makes their structure difficult to detect. Third, for Fe/Co−N_x materials, different kinds of active sites may contribute to the overall catalytic activity, even in one single type of material.[10] Despite the many debates that exist on these issues, the following consensuses have been reached regarding Fe/Co−N_x materials:[11] (i) the simultaneous presence of a transition metal and nitrogen plays an important role in the formation of active sites of the catalysts; (ii) nitrogen is a crucial component in the active sites; and (iii) the catalysts prepared with Co- or Fe-containing precursors are more active than those that use other transition metal (nonprecious metal) precursors.

Because the active site structure of Fe/Co−N_x materials after heat treatment is not yet clearly understood, it has proven to be difficult to determine the oxygen reduction mechanism. Some electroconductive polymers have been used as ligands to synthesize a new class of both pyrolyzed and nonpyrolyzed metal-doped polymer complex catalysts, owing to the high porosity, conductivity, and large effective area of such polymers.[5,12−20] It has also been reported that nonpyrolyzed cobalt−polypyrrole has a high ORR activity, without showing any noticeable loss of performance during operation of the PEFC.[5] Polyaniline is another kind of electroconductive polymer. Although a Fe−PANI catalyst prepared by heat treatment is described in the literature, it remains of interest to study nonpyrolyzed Fe/Co−PANI as an ORR catalyst for several reasons: first, the metal−PANI ligand structure might be determined so that the ORR mechanism could be simulated, which may lead to the discovery of the catalytic process in other Fe/Co−N_x materials; second, the synergistic effect between double metals (Fe and Co), which improves the ORR catalytic activity, could be studied with such a model, and third, the Fe/Co−PANI may potentially be a powerful catalyst for ORRs.

To shed light on the origin of their catalytic activity and the nature of their active sites, four kinds of metal−polyaniline molecular fragments were constructed, namely, Co−PANI, Fe−PANI, FeFe−PANI, and CoFe−PANI, and their ORR mechanism was investigated by way of density functional theory (DFT). The results indicate that the doping of monometal−polyaniline with another transition metal might enhance its catalytic activity somewhat.

Received: July 16, 2012
Revised: October 4, 2012
Published: October 8, 2012

dx.doi.org/10.1021/jp307055j | J. Phys. Chem. C 2012, 116, 22737−22742

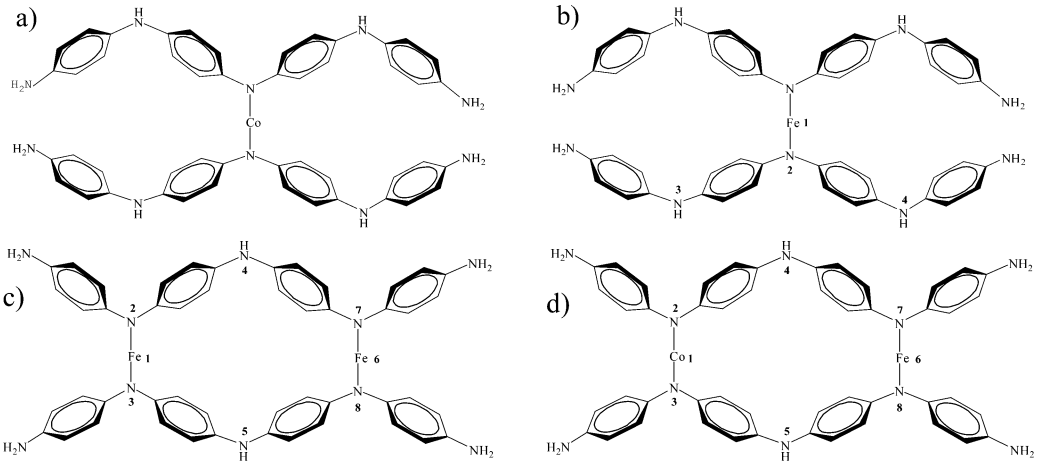

Figure 1. Schematic representation of metal−polyaniline molecular fragments: (a) Co−PANI, (b) Fe−PANI, (c) FeFe−PANI, and (d) CoFe−PANI.

2. COMPUTATIONAL METHODS

DFT calculations were carried out using the Amsterdam Density Functional program package (ADF, version 2010.01).[21−23] All oxygen reduction steps in the system were performed using the Becke (exchange) and the Lee−Yang−Parr (correlation)[24] functional (BLYP). The metal atoms, cobalt and iron, were modeled with a triple-ζ polarized (TZP) slater-type basis set, whereas other atoms were based on double-ζ polarized (DZP) sets. This method of mixing basis sets of different sizes is consistent with Ribas and Dragonetti's works,[25,26] which used TZP basis set for metal atom and DZP for nonmetallic atoms. Furthermore, Michalak's work also confirmed that the basis set effect for such systems is clearly very small.[27] The inner core orbitals, 1s for C, N, and O and 1s−3p for Co and Fe, were kept frozen. All atoms were allowed to relax without constraint in the geometry optimizations. For all stationary states, spin multiplicity was allowed to relax: possible geometries with varying spin states were carefully checked, and the ground state was determined to be the one with the lowest electronic energy. Furthermore, the atomic charges were obtained via multipole derived charge analysis (MDC-q),[28] which yields charges that reproduce (by construction) both the atomic and the molecular multipoles.

The chemical potential (the free energy per H atom) for the reaction ($H^+ + e^-$) can be derived from that of 1/2 H_2 in the gaseous phase by use of the standard hydrogen electrode model.[29−31] Therefore, under standard conditions (U = 0, pH 0, p = 1 bar, T = 298 K), the free-energy difference in the reaction of type *AH → A + H^+ + e^- may be calculated from the free energy in the reaction given by *AH → A + 1/2H_2. The change in free energy for a reaction is calculated using $\Delta G = \Delta E + \Delta ZPE - T\Delta S$, where ΔE is the reaction energy, ΔZPE is the difference in zero point energy, T is temperature, and ΔS is the change in entropy. In our work, the values of ΔE and ΔZPE were calculated via DFT, whereas the value for entropy is taken from a chemical database.[32]

Four metal−polyaniline molecular fragments were constructed to simulate the oxygen reduction mechanism of a catalyst (Figure 1). In each model, the metal atom is directly bonded to two polyaniline chains, thus generating a metal−N_x active site. The structural models of Co− and Fe−PANI are based on ref 16. The other two structural models, FeFe− and CoFe−PANI, are studied to estimate the synergistic effect between the two metal atoms, as evidenced by their higher catalytic performance.

3. RESULTS AND DISCUSSION

3.1. Stability Study. To evaluate the stability of the selected model structures, we calculated the energy change (ΔE) for the reactions between hydrated metal ions and polyaniline, as shown below. As is well-known, Co(II) and Fe(II) ions are both coordinated with six water molecules in solution.[32] For an exothermic reaction (a negative heat value), the calculations suggest that the metal−polyaniline structure is more energy favorable than the structure involving hydrated metal ions. The calculated results are listed in Table 1.

$$2(H - PANI_4) + [Co(H_2O)_6]^{2+} \rightarrow PANI_4 - Co - PANI_4 + 2[H_3O^+(H_2O)_2] \quad (1)$$

$$2(H - PANI_4) + [Fe(H_2O)_6]^{2+} \rightarrow PANI_4 - Fe - PANI_4 + 2[H_3O^+(H_2O)_2] \quad (2)$$

$$2(2H - PANI_4) + 2[Fe(H_2O)_6]^{2+} \rightarrow PANI_4 - FeFe - PANI_4 + 4[H_3O^+(H_2O)_2] \quad (3)$$

$$2(2H - PANI_4) + [Co(H_2O)_6]^{2+} + [Fe(H_2O)_6]^{2+} \rightarrow PANI_4 - CoFe - PANI_4 + 4[H_3O^+(H_2O)_2] \quad (4)$$

Table 1. Calculated Reaction Energies

structure	system	ΔE (eV)
Co−PANI	$PANI_4$−Co−$PANI_4$	−1.42
Fe−PANI	$PANI_4$−Fe−$PANI_4$	−0.91
FeFe−PANI	$PANI_4$−FeFe−$PANI_4$	−1.78
CoFe−PANI	$PANI_4$−CoFe−$PANI_4$	−2.11

From Table 1, it can be seen that each reaction has a negative ΔE value, indicating that all calculated reactions are exothermic. In other words, the selected metal−polyaniline structures are more stable than their hydrated metal ions.

3.2. Oxygen Adsorption. The generally sluggish ORR kinetics are due to the high strength of the O−O bond; the function of the catalyst is to facilitate the dissociation of that

dx.doi.org/10.1021/jp307055j | J. Phys. Chem. C 2012, 116, 22737−22742

bond. Therefore, the catalyst's ability to interact with oxygen is essential to its catalytic activity. If the interaction between the catalyst and oxygen (the metal−O interaction) is very weak, then the coverage of oxygen may be too low to allow for a high reaction rate. If oxygen bonds too strongly with the catalyst, then it will poison the surface and reduce its activity.

In general, there are two dioxygen adsorption modes: end-on and side-on. In this work, for each of the four metal−polyaniline models, the two adsorption modes are both calculated and their structures are fully optimized (Figure 2).

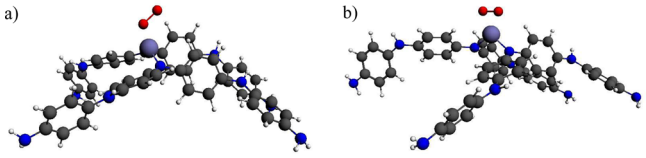

Figure 2. Structure of dioxygen adsorbed on Fe−PANI with (a) end-on mode and (b) side-on mode. The blue-gray circle is an iron atom, the blue circles are nitrogen atoms, the gray circles are carbon atoms, the red circles are oxygen atoms, and the small light circles are hydrogen atoms.

The calculation results suggest that the electronic energy for the side-on adsorption is lower than that for the end-on adsorption (for example, for Fe−PANI, the side-on adsorption energy is lower by ~0.96 eV than that for the end-on adsorption), which indicates that the side-on adsorption is more stable than the end-on type. As a result, the side-on adsorption modes are adopted.

To simplify the discussion, the initial states of Co−, Fe−, FeFe−, and CoFe−PANI are specified as A_0, B_0, C_0, and D_0, respectively. When O_2 is adsorbed on the active site, the corresponding states are named as A_1, B_1, C_1, and D_1. For Fe−PANI, one finds that O_2 is adsorbed in a configuration that is nearly side-on. (See Table 2.) This is due to a steric hindrance

Table 2. Calculated Equilibrium Internuclear Distances, *R* (Å), for Co−, Fe−, FeFe−, and CoFe−PANI

molecule	$R(Me-O_a)$	$R(M_e-O_b)$	$R(O_a-O_b)$
Co−PANI	1.830	1.885	1.416
Fe−PANI	1.836	1.842	1.441
FeFe−PANI	1.835	1.844	1.444
CoFe−PANI	1.776	1.938	1.442

effect that is a result of the geometry of Fe−PANI, where one of the aniline rings blocks the O_2 from freely approaching the Fe atom at the center of the aniline rings and thus prevents O_2 from forming a complete side-on configuration. The situation is nearly the same in the other three models. For Fe−PANI, the change in the Gibbs free energy (ΔG) associated with O_2 adsorption is about −1.37 eV, and the shortest distance between the Co atom and one O atom is 1.836 Å. When an O_2 molecule is adsorbed on the Fe−PANI surface, the O−O bond length is elongated from an equilibrium value of 1.245 to 1.441 Å, indicating that the molecular oxygen has been activated by the catalyst. This value is significantly higher than the elongations obtained for O_2 adsorption on metallophthalocyanine or metallooporphyrin, where O_2 is adsorbed in the end-on configuration.[33] This is because the strength of the O−O bond for the side-on configuration is generally weaker than that for the end-on configuration because of an increased d−π^* orbital overlap between metal and O_2 molecule.[34]

The calculated bond lengths of O_2 molecules in states A_1, C_1, and D_1 are 1.416, 1.444, and 1.442 Å, respectively. In the four metal−PANI models, the Fe−, FeFe−, and CoFe−PANI perform the O_2 bond elongations to nearly the same degree, all of them longer than that of Co−PANI. The free-energy change for O_2 in CoFe−PANI is −0.75 eV, which is the lowest of the four models. (The O_2 molecule is adsorbed on the surface of Fe atom because the highest occupied molecular orbital is mainly composed of Fe atom in CoFe−PANI's structure.) The data above indicate that the first electron-transfer step on Co− and Fe−PANI may be somewhat difficult due to the stronger adsorption of O_2.[26] In other words, the first oxygen reduction step on CoFe−PANI is more energy favorable than in each one of the other models.

3.3. Potential Energy Surface Profile for ORR. Potential energy surface profile is a useful method to evaluate the mechanism of ORR.[35] In the present study, the following oxygen reduction steps were modeled.

$$A_0 + O_2 \rightarrow A_0 - O_2(A_1) \quad (5)$$

$$A_0 - O_2 + H^+ + e^-(U) \rightarrow A_0 - OOH(A_2) \quad (6)$$

$$A_0 - OOH + H^+ + e^-(U) \rightarrow A_0 - OH - OH(A_3) \quad (7)$$

$$A_0 - OH - OH + H^+ + e^-(U) \rightarrow A_0 - OH + H_2O(A_4) \quad (8)$$

$$A_0 - OH + H^+ + e^-(U) \rightarrow A_0 - OH_2(A_5) \quad (9)$$

$$A_0 - OH_2 \rightarrow A_0 + H_2O \quad (10)$$

If the free energy of $A_0 + O_2 + 4(H^+ + e^-)$, $B_0 + O_2 + 4(H^+ + e^-)$, $C_0 + O_2 + 4(H^+ + e^-)$, and $D_0 + O_2 + 4(H^+ + e^-)$ is specified as 0 eV, then the relative free energies of $A_1(B_1, C_1, D_1) + 4(H^+ + e^-)$, $A_2(B_2, C_2, D_2) + 3(H^+ + e^-)$, $A_3(B_3, C_3, D_3) + 2(H^+ + e^-)$, $A_4(B_4, C_4, D_4) + H_2O + (H^+ + e^-)$, and $A_5(B_5, C_5, D_5) + H_2O$ are illustrated in the energy profile shown in Figure 3.

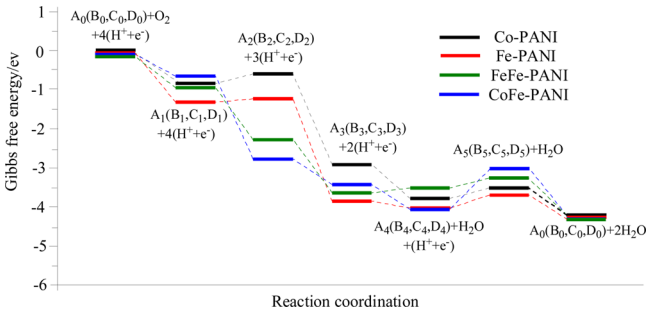

Figure 3. Potential energy surface profiles for O_2 reduction in the four reaction systems.

For the first O_2 reduction step (eq 6), the values of ΔG are 0.26 and 0.13 eV for Co− and Fe−PANI, respectively (Figure 3), indicating that they are both endergonic. For FeFe− and CoFe−PANI, the ΔG values are −1.24 and −2.13 eV, which indicates that CoFe−PANI is the most energy favorable arrangement.

dx.doi.org/10.1021/jp307055j | J. Phys. Chem. C 2012, 116, 22737−22742

The second oxygen reduction step (eq 7) is the key step that breaks the bond between dioxygen, and −OOH is not reduced to H_2O_2 but rather to two −OH, as shown in Figure 4. This is

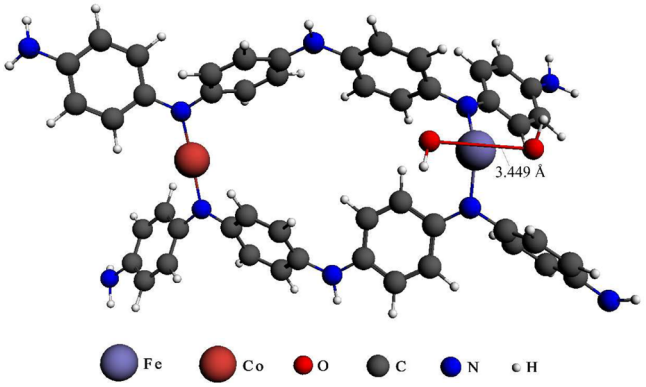

Figure 4. Optimized structures of state D_3 (CoFe−PANI−OH−OH).

quite different from what happens in reactions involving metallophthalocyanine, metalloporphyrin, and cobalt−polypyrrole,[36] which are all reduced to an adsorbed oxygen and one H_2O molecule (−OOH + H^+ + e^-→ −O + H_2O). The implication is that the metal−PANIs may have a strong interaction with the adsorbed −OH.

The last oxygen reduction step (eq 9) is endergonic. It is very unfavorable and perhaps induces an overpotential, as discussed in the next section.

3.4. Adsorption Properties of Intermediates. The adsorption energies of the intermediates in the dioxygen reduction steps are listed in Table 3. The one with the strongest

Table 3. Calculated Adsorption Energies, AE (eV), in the Sum of O_2 Reduction Steps for Co−, Fe−, FeFe−, and CoFe−PANI

molecule	AE(O)	AE(OH)	AE(OOH)
Co−PANI	−4.36	−3.01	−1.63
Fe−PANI	−4.55	−3.30	−2.27
FeFe−PANI	−4.58	−2.89	−3.25
CoFe−PANI	−4.92	−3.32	−3.91

adsorption energy of −O is found with CoFe−PANI, where the energy is −4.92 eV. It is close to that of an −O adsorbed at the edge between the (111) and (100) facets on a 1 nm Pt cluster (−4.87 eV).[37] For the Fe−PANI (FeFe−PANI), the adsorption energy of −O is −4.55 eV, which is weaker by 0.37 eV when compared with that in CoFe−PANI and which is very close to the adsorption energy on the Pt (111) surface (−4.54 eV).[37] For Co−FANI, we find the adsorption energy is −4.36 eV, the smallest of the lot. Xu et al. postulate that the stronger the bond formation between catalyst and atomic oxygen, the more powerful the catalyst will be in breaking the bond in molecular oxygen.[38] Therefore, from that perspective, the catalytic activity levels should decrease in the sequence CoFe−PANI> Fe−PANI (FeFe−PANI) > Co−PANI.

The adsorption energies for −OH and −OOH on the four metal−PANIs are listed in Table 3, where it can be seen that CoFe−PANI presents the strongest adsorption for the two oxygen reduced intermediates, which manifests as an −O adsorption.

Table 4 shows the net atomic charges for the entire O_2 reduction intermediates as produced by MDC-q population analyses. Among the four models, the intermediate species catalyzed by CoFe−PANI accumulate the most negative charges. This clearly implies that within a certain range the large net charge of the adsorbed intermediates could induce a high adsorption strength, and the high adsorption strength in turn could result in a high level of catalytic activity.

Experimental results indicate that the strong −OH adsorption on Pt may cause an overpotential,[39] because the −OH might cover the Pt surface and block the adsorption of molecular oxygen in the subsequent step. In the final oxygen reduction step (eq 9), which is catalyzed by a metal−PANI, additional externally supplied energy would be needed to complete the −OH reduction process, especially for CoFe−PANI (see Figure 3). Therefore, although the CoFe−PANI has the highest catalytic activity among the four catalysts, the possibility of an overpotential caused by strong −OH adsorption may weaken its catalytic behavior.

3.5. Synergistic Effect. As discussed above, when the electron-withdrawing group (−OO, −OOH, −O, or −OH) is adsorbed on the active site, an electron flows from the catalyst molecule to the group (see Table 4). For Fe−PANI, the maximum change in charge (absolute value) for iron in the ORR is ∼21%, as illustrated in Figure 5 a, and for each nitrogen (in one of the aniline chains) the change is <15%, implying that the electrons extracted by the adsorbed groups are mainly contributed by the iron atom.

For the ORR catalyzed by CoFe−PANI, the situation is quite different. As shown in Figure 5 b, the maximum change in charge for Fe(6) is ∼28%, which is larger than that found in Fe−PANI. For the Co(1) atom, this change is much more obvious. The maximum charge-changing for Co(1) is as high as 48%, whereas that for each nitrogen is <25%. The data indicate that in CoFe−PANI the cobalt atom could directly donate its electron to iron through the closed-ring that consists of Co(1), N(2), N(3), N(4), N(5), Fe(6), N(7), and N(8). By contrast, the electron transfer between the homogeneous metal atoms in FeFe−PANI is obviously weaker than that in CoFe−PANI. The synergistic effect between these heterogeneous metal atoms could explain why the catalytic intermediates on CoFe−PANI can carry more negative charges than those in the other metal−PANIs.

The energy gaps between the highest occupied molecular orbital (HOMO) and the lowest unoccupied molecular orbital (LUMO) in Co−, Fe−, FeFe−, and CoFe−PANI are 0.502, 0.388, 0.380, and 0.348 eV, respectively. In general, if a

Table 4. Calculated MDC-q Charges, ΔQ, in the Sum of O_2 Reduction Steps for Co−, Fe−, FeFe− and CoFe−PANI

molecule	$\Delta Q(O_2)$	ΔQ(OOH)	ΔQ(OH−OH)	ΔQ(OH)	$\Delta Q(H_2O)$
Co−PANI	−0.482	−0.268	−0.631	−0.327	0.099
Fe−PANI	−0.515	−0.501	−0.641	−0.393	0.080
FeFe−PANI	−0.521	−0.604	−0.642	−0.387	0.025
CoFe−PANI	−0.538	−0.629	−0.648	−0.401	0.015

dx.doi.org/10.1021/jp307055j | J. Phys. Chem. C 2012, 116, 22737−22742

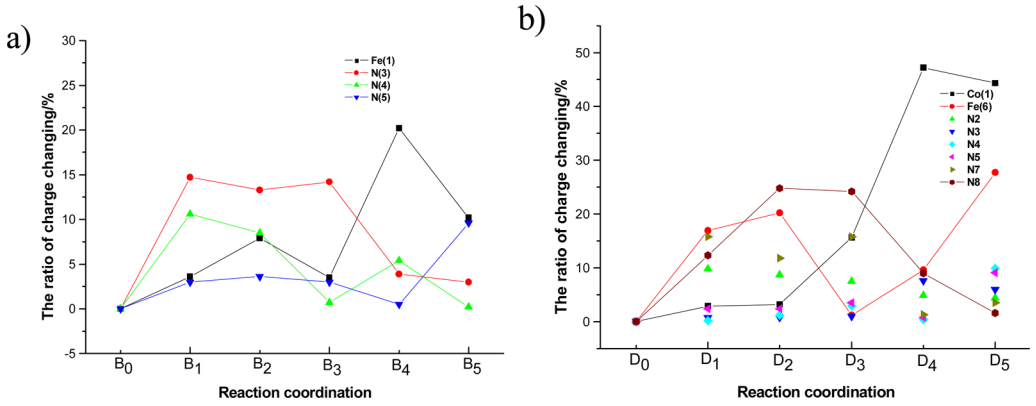

Figure 5. Ratio of change in charge for the sum of reaction steps from B_0–B_5 for (a) Fe–PANI and from D_0 to D_5 for (b) CoFe–PANI. Atoms are numbered according to Figure 1.

molecule has a large HOMO–LUMO gap (HLG), then it should be very inert and stable.[40] Conversely, a smaller HLG implies lower kinetic stability and higher chemical reactivity, because it is energetically favorable to add electrons to a low-lying LUMO or to receive electrons from a high-lying HOMO and thus to form the activated complex in any potential reaction.[41] Among the four metal–PANIs, the CoFe–PANI has the smallest HLG because the participation of a Co atom decreases the HLG of CoFe–PANI. That is to say, the CoFe–PANI is more active than the FeFe–PANI owing to the electron transfer from a metal 3d orbital to the π^* orbital of an oxygen molecule. This conclusion is also confirmed by an analysis of the HOMO and LUMO orbitals. The orbital energy levels for CoFe–PANI and FeFe–PANI are shown in Figure 6,

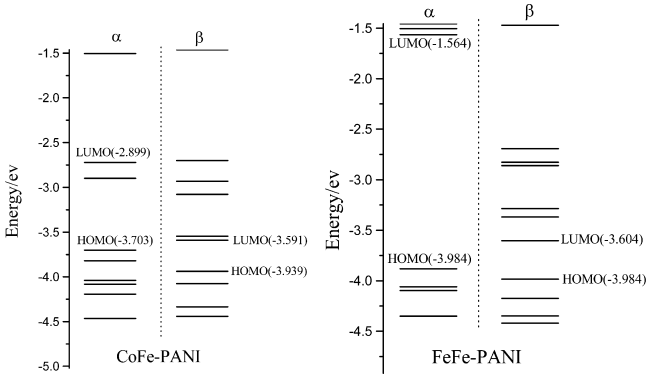

Figure 6. Energy levels in CoFe–PANI and FeFe–PANI (α = spin-up orbital; β = spin-down orbital).

where it appears that the HOMO energy levels for both spin-up and spin-down orbitals in CoFe–PANI are all higher than the corresponding levels in FeFe–PANI. This suggests that the doped cobalt might not only serve to decrease the HLG but also to enhance the HOMO level and thus facilitate electron transfer. On the basis of the HLG values, we conclude that Co–PANI is the most inactive catalyst among the four models. The ordering of the sequence of catalytic activity is confirmed once more and is consistent with the result obtained by the adsorption analysis for the oxygen reduction intermediates.

In CoFe–PANI, fluctuations in the d-orbital configuration are induced by the presence of double metals (Fe and Co), which might further enhance the catalytic activity. This idea may be applied to other Fe/Co–N_x materials to achieve improved activity levels.

4. CONCLUSIONS

A detailed investigation of oxygen reduction steps catalyzed by metal–polyaniline has been performed using DFT. The results indicate that the dioxygen absorption mode is determined not only by the center metal but also by the steric hindrance. In the ORR process, it is found that –OH, not H_2O_2, plays the role of intermediate. The catalytic activities for the models under investigation decrease in the sequence CoFe–PANI > Fe–PANI (FeFe–PANI) > Co–PANI. This is the result of a synergistic effect between the heterogeneous metal atoms in CoFe–PANI, which allows it to donate additional electrons from the active site to the adsorbed oxygen reduction intermediates. The doping of cobalt could also decrease the HOMO–LUMO gap in CoFe–PANI and thus make it more active.

AUTHOR INFORMATION

Corresponding Author

*Tel: +86 10 67396158. Fax: +86 10 67391983. E-mail: sunsr@bjut.edu.cn (S.S.), dgxia@pku.edu.cn (D.X.).

Notes

The authors declare no competing financial interest.

ACKNOWLEDGMENTS

This work was performed with the financial support from the Fundamental Science Research Foundation of Beijing University of Technology (X4005012201101), the major program of Beijing Municipal Natural Science Foundation (no. 20110001), and National Natural Science Foundation of China (no. 11179001).

REFERENCES

(1) Gasteiger, H. A.; Kocha, S. S.; Sompalli, B.; Wagner, F. T. *Appl. Catal., B* **2005**, *56*, 9–35.

(2) Borup, R.; Meyers, J.; Pivovar, B.; Kim, Y. S.; Mukundan, R.; Garland, N.; Myers, D.; Wilson, M.; Garzon, F.; Wood, D.; et al. *Chem. Rev.* **2007**, *107*, 3904–3951.

(3) Lefèvre, M.; Proietti, E.; Jaouen, F.; Dodelet, J. P. *Science* **2009**, *324*, 71–74.

(4) Jaouen, F.; Proietti, E.; Lefèvre, M.; Chenitz, R.; Dodelet, J. P.; Wu, G.; Chung, H. T.; Johnston, C. M.; Zelenay, P. *Energy. Environ. Sci.* **2011**, *4*, 114–130.

(5) Bashyam, R.; Zelenay, P. *Nature* **2006**, *443*, 63–66.

(6) Ikeda, T.; Boero, M.; Huang, S. F.; Terakura, K.; Oshima, M.; Ozaki, J. *J. Phys. Chem. C* **2008**, *112*, 14706−14709.
(7) Matter, P. H.; Zhang, L.; Ozkan, U. S. *J. Catal.* **2006**, *239*, 83−96.
(8) Maldonado, S.; Morin, S.; J. Stevenson, K. *Carbon* **2006**, *44*, 1429−1437.
(9) Subramanian, N. P.; Li, X.; Nallathambi, V.; Kumaraguru, S. P.; Colon-Mercado, H.; Wu, G.; Lee, J. W.; Popov, B. N. *J. Power Sources* **2009**, *188*, 38−44.
(10) Chlistunoff, J. *J. Phys. Chem. C* **2011**, *115*, 6496−6507.
(11) Li, X.; Liu, G.; Popov, B. N. *J. Power Sources* **2010**, *195*, 6373−6378.
(12) Asazawa, K.; Yamada, K.; Tanaka, H.; Oka, A.; Taniguchi, M.; Kobayashi, T. *Angew. Chem; Int. Ed.* **2007**, *46*, 8024−8027.
(13) Qin, H. Y.; Liu, Z. X.; Yin, W. X.; Zhu, J. K.; Li, Z. P. *J. Power Sources* **2008**, *185*, 909−912.
(14) Wu, G.; More, K. L.; Johnston, C. M.; Zelenay, P. *Science* **2011**, *332*, 443−447.
(15) Han, S. J.; Jung, H. J.; Shim, J. H.; Kim, H. C.; Sung, S. J.; Yoo, B.; Lee, D. H.; Lee, C.; Lee, Y. *J. Electroanal. Chem.* **2011**, *655*, 9−44.
(16) Millán, W. M.; Thompson, T. T.; Arriaga, L. G.; Smit, M. A. *Int. J. Hydrogen Energy* **2009**, *34*, 694−702.
(17) Sulub, S. R.; Millán, W. M.; Smit, M. A. *Int. J. Electrochem. Sci.* **2009**, *4*, 1015−1027.
(18) Wu, G.; Nelson, M. A.; Mack, N. H.; Ma, S.; Sekhar, P.; Garzon, F. H.; Zelenay, P. *Chem. Commun.* **2010**, *46*, 7489−7491.
(19) Wu, G.; Johnston, C. M.; Mack, N. H.; Artyushkova, K.; Ferrandon, M.; Nelson, M.; Lezama-Pacheco, J. S.; Conradson, S. D.; More, K. L.; Myers, D. J.; et al. *J. Mater. Chem.* **2011**, *21*, 11392−11405.
(20) Wu, G.; Nelson, M.; Ma, S.; Meng, H.; Cui, G.; Shen, P. K. *Carbon* **2011**, *49*, 3972−3982.
(21) te Velde, G.; Bickelhaupt, F. M.; Baerends, E. J.; Fonseca Guerra, C.; van Gisbergen, S. J. A.; Snijders, J. G.; Ziegler, T. *J. Comput. Chem.* **2001**, *22*, 931−967.
(22) Fonseca Guerra, C.; Snijders, J. G.; te Velde, G.; Baerends, E. J. *Theor. Chem. Acc.* **1998**, *99*, 391−403.
(23) *ADF2010.01, SCM, Theoretical Chemistry*; Vrije Universiteit: Amsterdam, The Netherlands. http://www.scm.com.
(24) Lee, C.; Yang, W.; Parr, R. G. *Phys. Rev. B* **1988**, *37*, 785−789.
(25) Ribas, X.; Xifra, R.; Parella, T.; Poater, A.; Solà, M.; Llobet, A. *Angew. Chem.; Int. Ed.* **2006**, *45*, 2941−2944.
(26) Dragonetti, C.; Righetto, S.; Roberto, D.; Ugo, R.; Valore, A.; Fantacci, S.; Sgamellotti, A.; Angelis, F. D. *Chem. Commun.* **2007**, *40*, 4116−4118.
(27) Michalak, A.; DeKock, R. L.; Ziegler, T. *J. Phys. Chem. A* **2008**, *112*, 7256−7263.
(28) Swart, M.; van Duijnen, P. Th.; Snijders, J. G. *J. Comput. Chem.* **2001**, *22*, 79−88.
(29) Nørskov, J. K.; Rossmeisl, J.; Logadottir, A.; Lindqvist, L.; Kitchin, J. R.; Bligaard, T.; Jonsson, H. *J. Phys. Chem. B* **2004**, *108*, 17886−17892.
(30) Karlberg, G. S.; Rossmeisl, J.; Norskov, J. K. *Phys. Chem. Chem. Phys.* **2007**, *9*, 5158−5161.
(31) Sun, S.; Jiang, N.; Xia, D. *J. Phys. Chem. C* **2011**, *115*, 9511−9517.
(32) Wang, Z. L.; Zhou, Y. P. *Physical Chemistry*, 4th ed.; Higher Education Press: Beijing, China, 2007.
(33) Dipojono, H. K.; Saputro, A. G.; Belkada, R.; Nakanishi, H.; Kasai, H.; David, M.; Dy, E. S. *J. Phys. Soc. Jpn.* **2009**, *78*, 094710.
(34) Tsuda, M.; Dy, E. S.; Kasai, H. *J. Chem. Phys.* **2005**, *122*, 244719.
(35) Zhang, L. P.; Xia, Z. H. *J. Phys. Chem. C* **2011**, *115*, 11170−11176.
(36) Chen, X.; Li, F.; Wang, X.; Sun, S.; Xia, D. *J. Phys. Chem. C* **2012**, *116*, 12553−12558.
(37) Han, B. C.; Miranda, C. R.; Ceder, G. *Phys. Rev. B* **2008**, *77*, 075410.
(38) Xu, Y.; Ruban, A. V.; Mavrikakis, M. *J. Am. Chem. Soc.* **2004**, *126*, 4717−4725.
(39) Uribe, F. A.; Zawodzinski, T. A. *Electrochim. Acta* **2002**, *47*, 3799−3806.
(40) Li, J.; Li, X.; Zhai, H. J.; Wang, L. S. *Science* **2003**, *299*, 864−867.
(41) Kim, K. H.; Han, Y. K.; Jung, J. *Theor. Chem. Acc.* **2005**, *113*, 233−237.